

UC Berkeley

UC Berkeley Previously Published Works

Title

Nuclear Pore Permeabilization Is a Convergent Signaling Event in Effector-Triggered Immunity

Permalink

<https://escholarship.org/uc/item/7hk11771>

Journal

Cell, 166(6)

ISSN

0092-8674

Authors

Gu, Yangnan
Zebell, Sophia G
Liang, Zizhen
[et al.](#)

Publication Date

2016-09-01

DOI

10.1016/j.cell.2016.07.042

Peer reviewed



Published in final edited form as:

Cell. 2016 September 8; 166(6): 1526–1538.e11. doi:10.1016/j.cell.2016.07.042.

Nuclear Pore Permeabilization Is a Convergent Signaling Event in Effector-Triggered Immunity

Yangnan Gu¹, Sophia G. Zebell¹, Zizhen Liang², Shui Wang³, Byung-Ho Kang², and Xinnian Dong^{1,*}

¹Howard Hughes Medical Institute-Gordon and Betty Moore Foundation, Department of Biology, PO Box 90338, Duke University, Durham, North Carolina 27708, USA

²School of Life Sciences, Center for Cell and Developmental Biology and State Key Laboratory of Agrobiotechnology, The Chinese University of Hong Kong, Hong Kong, China

³Development Center of Plant Germplasm Resources, College of Life and Environmental Sciences, Shanghai Normal University, Shanghai 200234, China

SUMMARY

Nuclear transport of immune receptors, signal transducers, and transcription factors is an essential regulatory mechanism for immune activation. Whether and how this process is regulated at the level of the nuclear pore complex (NPC) remains unclear. Here we report that CPR5, which plays a key inhibitory role in effector-triggered immunity (ETI) and programmed cell death (PCD) in plants, is a novel transmembrane nucleoporin. CPR5 associates with anchors of the NPC selective barrier to constrain nuclear access of signaling cargos and sequesters Cyclin-dependent Kinase Inhibitors (CKIs) involved in ETI signal transduction. Upon activation by immunoreceptors, CPR5 undergoes an oligomer to monomer conformational switch, which coordinates CKI release for ETI signaling and reconfigures the selective barrier to allow significant influx of nuclear signaling cargos through the NPC. Consequently, these coordinated NPC actions result in simultaneous activation of diverse stress-related signaling pathways and constitute an essential regulatory mechanism specific for ETI/PCD induction.

Graphical Abstract

*Correspondence should be addressed to: X.D. (xdong@duke.edu).

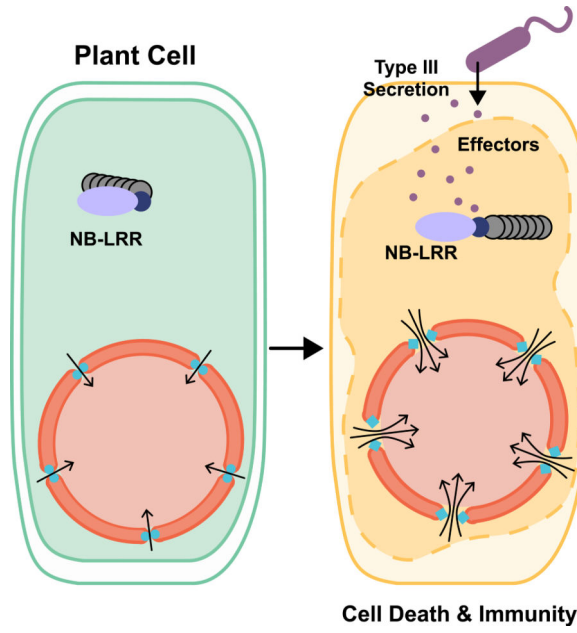
Publisher's Disclaimer: This is a PDF file of an unedited manuscript that has been accepted for publication. As a service to our customers we are providing this early version of the manuscript. The manuscript will undergo copyediting, typesetting, and review of the resulting proof before it is published in its final citable form. Please note that during the production process errors may be discovered which could affect the content, and all legal disclaimers that apply to the journal pertain.

SUPPLEMENTAL INFORMATION

Supplemental information includes six figures and two tables and can be found with this article online at XXX.

AUTHOR CONTRIBUTIONS

Y.G., S.W., and X.D. designed the research. Y.G. performed most of the experiments. S.G.Z contributed dataset GSE72742. Z.L. and B.K. performed the immunoelectron microscopy. S.W. helped with the protein complex purification. Y.G. and X.D. wrote the paper with comments from all authors.



INTRODUCTION

Effector-triggered immunity (ETI) is a vital mechanism for host recognition of pathogen virulence effectors to trigger defense (Jones and Dangl, 2006; Stuart et al., 2013). In plants, ETI is activated by nucleotide-binding leucine-rich repeat (NB-LRR) receptors, which are divided into two major classes based on the presence of an N-terminal coiled-coil (CC) domain or a Toll-interleukin1 receptor (TIR) domain. NB-LRRs have been found to localize in various subcellular compartments, where they can detect activities of different pathogen effectors (Elmore et al., 2011). Although quantitative differences exist in outcomes of ETI mediated by different NB-LRRs, they all result in similar transcriptional reprogramming of the infected cells, which leads to restriction of pathogen growth and rapid programmed cell death (PCD). This suggests a common cellular regulatory mechanism connecting distinct NB-LRR activation events to a unified transcriptional response in the nucleus.

Genetic and molecular studies have shown that changes in the nucleocytoplasmic dynamics of NB-LRR receptor complexes, signal transducers and immune-related transcriptional regulators are crucial for defense gene expression and resistance during ETI (Garcia and Parker, 2009; Rivas, 2012). Screens for suppressors of an autoactivated TIR-NB-LRR protein mutant, *snc1*, led to the identification of *mos* (*modifiers of snc1*) mutants, including two (*mos3* and *mos7*) in the nuclear pore complex (NPC) and one (*mos6*) in a nuclear transport receptor (NTR) (Cheng et al., 2009; Palma et al., 2005; Zhang and Li, 2005). These and other evidence suggested that the NPC- and NTR-directed nucleocytoplasmic transport are involved in subcellular defense coordination triggered by NB-LRRs (Wirthmueller et al., 2013). However, because these *mos* and other nucleoporin mutants are also compromised in resistance independent of NB-LRRs (Wiermer et al., 2012), whether the NPC plays a generic role in mediating transport of defense signals or a specific regulatory role for distinct immune mechanisms remains unclear.

In contrast to the *mos* mutants, which block immune responses, loss-of-function mutations in the putative nuclear envelope (NE) protein CPR5 (Constitutive Expresser of PR Genes 5) result in an ETI-like transcriptome and PCD (Wang et al., 2014). Consequently these mutants show resistance against multiple pathogens carrying effectors independent of cognate NB-LRR receptors (Boch, 1998; Bowling et al., 1997). These evidence suggest that CPR5 regulates an essential downstream inhibitory mechanism of ETI/PCD, possibly at the nucleocytoplasmic barrier.

We previously showed that two Cyclin-dependent Kinase Inhibitors (CKIs), SIM (SIAMESE) and SMR1 (SIAMESE-Related 1), are redundantly required for downstream ETI/PCD signaling in the *cpr5* mutant. CPR5 sequesters CKIs in the NE and specifically releases them in response to NB-LRR activation to engage the Retinoblastoma (Rb) and the E2F-mediated cell cycle pathway to regulate defense gene expression and PCD (Wang et al., 2014). However, how are CKIs released remains unknown. Moreover, whether redirection of the cell cycle pathway is sufficient for *cpr5*-mediated ETI/PCD needs further investigation.

In this study, we report that CPR5 is a plant transmembrane nucleoporin that physically associates with the NPC core scaffold. CPR5 resides in the NPC as a homomeric complex, which is specifically disrupted in response to NB-LRR activation. This conformational change in the NPC plays a dual role during ETI/PCD activation: it enables dissociation of CKIs from the NPC to engage cell cycle regulators for defense gene expression and reconfigures the NPC selective barrier to allow massive nuclear influx of diverse stress-related signaling cargos. These CPR5-coordinated actions of the NPC are required for ETI/PCD induction and constitute a downstream regulatory mechanism specific for NB-LRR-mediated ETI/PCD.

RESULTS

CPR5 Is a Transmembrane Protein Enriched in the Nuclear Pore

To define the molecular role of CPR5, we first determined its precise subcellular localization using a fusion to the green fluorescence protein (GFP-CPR5), which we have previously shown to be functional (Wang et al., 2014). Using both transient expression in *Nicotiana benthamiana* and stable expression in *Arabidopsis*, we found that CPR5 was exclusively associated with the endomembrane system, including the nuclear envelope (NE) and endoplasmic reticulum (ER)-associated large granules (Figures 1A, 1B, S1A and S1B). We next investigated its membrane targeting mechanism by first verifying its predicted transmembrane domains (TMDs). Using trypsin digestion followed by shotgun sequencing with mass spectrometry (MS), we found a highly biased peptide coverage pattern. In the conserved C-terminal region of AtCPR5, no peptide was detected within the predicted TMDs (Figures 1C and S1C), consistent with the MS profiling patterns found in other integral membrane proteins (Washburn et al., 2001). Null mutations within the TMDs (Bowling et al., 1997; Jing et al., 2007; Yoshida et al., 2002) (Figure 1C) and sequential deletions of TMDs from the C terminal end all caused the protein to be trapped in a tubular ER structure (Figures 1A, right panel, and 1D), highlighting the importance of these TMDs in functional targeting of the CPR5 protein.

Three-dimensional image reconstruction of the nuclear surface revealed that CPR5 was not distributed evenly in the NE, but enriched in punctate structures (Figures 1E and S1A, right panel). Distinct from the large mobile granules associated with the ER, these static puncta are smaller in size and densely distributed in the NE, resembling nuclear pores. Subsequent immunogold labeling of GFP-CPR5 followed by transmission electron microscopy (TEM) and tomography analyses confirmed that CPR5 is indeed associated with the NPC (Figures 1F and 1G). Structural integrity of the NPC is known to play a role in maintaining NE stability (Alber et al., 2007) and changes in levels of a number of NPC components (nucleoporins) cause NE membrane deformation (Jevtic et al., 2014). We found that prolonged overexpression of CPR5 could indeed elicit hypobulbated nuclei and inner nuclear speckles (Figure 1H), whereas loss of CPR5 resulted in abnormal spherical nuclei (Figures 1I and 1J), consistent with the NE morphology observed in multiple nucleoporin mutants (Parry, 2014; Parry et al., 2006; Tamura et al., 2010). In contrast to its NE localization, which clearly has a functional impact, CPR5-associated ER granules are distinct from any of the known membrane structures tested (Figures 1D and S1B). We hypothesize that this pool of CPR5 may represent a nonspecific membrane association due to overexpression.

CPR5 Is a Transmembrane Nucleoporin Associated with the NPC Core Scaffold

Proteomic analysis of the affinity-purified YFP-CPR5 protein complex identified a total of 28 potential binding partners of CPR5 (Figure S2A and S2B), which contain two functional groups that support our hypothesis of CPR5 being a membrane-bound nucleoporin (Figure 2A). The first group contains proteins which function in membrane protein synthesis and maturation. These interactors were likely captured by newly synthesized CPR5 protein in the ER on route to the NE. The second group consists two proteins, nucleoporin 155 (Nup155), a core scaffold component of NPC, and a putative cell cycle controlling phosphatase, both of which were previously identified as associated with the NPC in plants (Tamura et al., 2010). We subsequently verified that CPR5 and Nup155 interact specifically in the NPC using the Bimolecular Fluorescence Complementation (BiFC) assay (Figure 2B). In addition, a Fluorescence Recovery After Photobleaching (FRAP) assay indicated that CPR5 is anchored in the NE with low mobility, and thus likely forms a stable complex with Nup155 in the NPC (Figure 2C).

To gain further insight into the position of CPR5 within the NPC, we mapped the interactions of CPR5 with nucleoporins of different NPC subcomplexes. The core NPC contains eight copies of symmetric spokes, each consisting of interconnected subcomplexes: the outer ring complex (ORC) that coats the pore membrane, the inner ring complex (IRC) that forms the NPC core scaffold together with the ORC, the transmembrane ring (MR) that anchors the core scaffold to the pore membrane, and the linker nucleoporins that bridge the core scaffold and Phe-Gly (FG) proteins, which form the selective barrier for cargo transport (Alber et al., 2007). Using both BiFC *in planta* and an *in vitro* pull-down assay, we found that CPR5 interacts with not only Nup155 in the IRC but also the IRC-associated linker nucleoporin Nup93a through its N-terminus (Figures 2D and 2E). However, no robust interaction was detected with FG proteins, ORC components or other NPC accessory proteins tested (Figure 2D). Based on these observations, we propose that CPR5 is a

transmembrane nucleoporin that is anchored at the equatorial plane of the NPC in the nuclear pore membrane by its C-terminal TMDs and physically interacts with the NPC core scaffold as well as an associated linker nucleoporin through its soluble N-terminus (Figure 2F).

CPR5 Is Involved for NPC Function

Consistent with the notion of CPR5 being a nucleoporin, CPR5 displays strong genetic interactions with the ORC nucleoporins Nup85, Nup96 and Nup160. Whereas the *nup85*, *nup96* and *nup160* single mutants did not exhibit obvious aberrations in early seedling development, double mutants with *cpr5* all resulted in embryonic or seedling lethality (Figure 2G). This synergistic genetic relationship is likely due to a cooperative role between CPR5 and ORC components in maintaining the structural integrity of the NPC. We were unable to assess genetic interactions between CPR5 and IRC nucleoporins due to seedling or embryonic lethality of the single mutants (Parry, 2014).

Plants have sequence-homologs of almost all the vertebrate nucleoporins (Tamura et al., 2010). However, because transmembrane nucleoporins are not evolutionarily conserved (Mans et al., 2004), functional analogs of vertebrate transmembrane nucleoporins that interact with the IRC and anchor the NPC to the pore membrane have not been identified in plants. Our study suggests that CPR5 is a plant-specific transmembrane nucleoporin that physically associates with the IRC and may contribute to the stability of the NPC core scaffold even though it is not required for NPC anchoring (Figure S2C). Besides its potential structural role in the NPC, the *cpr5* mutant phenotype suggests that this plant transmembrane nucleoporin may have evolved distinct functions, such as regulation of ETI/PCD.

CPR5 Modulates the Nucleocytoplasmic Transport Activity of the NPC

The NPC is a platform for multiple nuclear activities, including nucleocytoplasmic transport, genome maintenance, and regulation of gene expression (Strambio-De-Castillia et al., 2010). To understand how CPR5 regulates ETI in the NPC, we first investigated the cellular processes controlled by this nucleoporin using transcriptome profiling. To avoid the indirect effects of the stable *cpr5* mutation, which is known to activate ETI as well as the downstream signaling pathways mediated by the immune signal salicylic acid (SA) (Bowling et al., 1997; Wang et al., 2014), a transient interference system was developed. Because of the low turnover rate of nucleoporins (Toyama et al., 2013), we designed a protein interference strategy that involved dexamethasone (dex)-inducible expression of the C-terminal half (275–564 aa) of CPR5 (CPR5-C). Although CPR5-C is not functional (Figure S3A), it is targeted to the NPC (Figure S3B) and therefore might compete with the wild type (WT) protein (Figure 3A). We first tested the system using a transient expression assay performed in *N. benthamiana*. We found that overexpression of CPR5-C led to tissue collapse similar to ETI-associated PCD induced by NB-LRR activation, whereas overexpression of the full-length CPR5 or CPR5-N had no such an effect (Figure S3C). This CPR5-C-induced PCD was likely due to interference with the function of endogenous CPR5 because it was suppressible by simultaneous overexpression of full-length CPR5, but not CPR5-N (Figure S3D). We subsequently validated the interference activity of YFP-CPR5-C

in *Arabidopsis*, where constitutive or inducible expression of YFP-CPR5-C in the WT background resulted in the *cpr5* mutant phenotypes, including growth arrest, PCD and increased expression of defense genes (Figure S3E–S3G).

The stable *Dex:YFP-CPR5-C* transgenic line was then used for transcriptome analysis. Using principal component analysis, we detected a major change in global gene expression 24 hours after YFP-CPR5-C was induced (Figure 3B), when SA-mediated response had yet to occur in this system (Figure S3H). About 1,800 differentially expressed genes (DEGs) were identified (Figure 3C and Table S1). Comparative analysis with 438 published *Arabidopsis* microarray datasets collected under the conditions of a broad spectrum of chemical/stress/hormone treatments (Reina-Pinto et al., 2010) revealed that the CPR5-C-induced transcriptome has significant matches with a variety of stress responses, especially to cold, salt/osmotic stress, abscisic acid, and various pathogens (Figure 3D). We also performed Gene Set Enrichment Analysis (GSEA) using a even more comprehensive database (Yi et al., 2013), which revealed a transcriptome feature composed of distinct molecular signatures, including activation of cold/dehydration/ABA responses and PHYB/CRY1-dependent light responses, and repression of gibberellin and auxin responses (Figures 3E and 3F). The significance of these molecular signatures was further supported by the enrichment of *cis*-elements known for these responses in total DEGs (Figure 3G).

Such a composite transcriptome profile is most likely due to perturbation of a key cellular process shared by these corresponding pathways instead of crosstalk effects induced by a single signaling pathway. Nucleocytoplasmic protein transport is a critical rate-limiting step for hormones and light signal transduction. Nuclear translocation of photoreceptors PHYs and CRY1 is required for activation of light responses, whereas nuclear accumulation of DELLA and Aux/IAA proteins results in repression of gibberellin and auxin signaling, respectively (Lee et al., 2008). Notably, a number of mutants with altered responses to cold, drought/ABA and auxin have been genetically identified as components of the NPC and NTRs (Dong et al., 2006; Lee et al., 2001; Parry et al., 2006; Verslues et al., 2006), illustrating the sensitivity of these processes to the structural integrity and/or transport activity of the nuclear pore. Indeed, ABA and auxin were the most sensitive pathways detected by a natural language processing (NLP)-based network regulator discovery algorithm when applied to the DEGs caused by CPR5-C interference (Figure 3C). We hypothesize that with compromised CPR5 function, the NPC adopts a structure with significantly increased permeability and/or transport activity that allows deregulated nuclear influx of diverse signaling cargos, which normally undergo nuclear translocation only under stimulus-induced conditions.

We next tested whether the WT CPR5 constrains the nuclear accumulation of signaling cargos. We found that overexpressing CPR5 indeed caused substantial cytoplasmic retention of stress- and hormone-related nuclear proteins NPR1, JAZ1 and ABI5 (Figures 4A, 4B, S4A and S4B). However, WIT1 (an NE protein), Nup155 or a mutant form of CPR5 (G420D) could not recapitulate this effect (Figures 4A, S4A and S4B), supporting a direct role for CPR5 in modulating nucleocytoplasmic transport activity of the NPC. Consistent with the cytoplasmic retention of these nuclear signaling molecules, overexpression CPR5

compromises ETI-associated PCD and resistance in *Arabidopsis* (Wang et al., 2014), suggesting that CPR5 is a direct rate-limiting regulator for ETI/PCD.

CPR5 Inhibits Immune Signal Transport through the Selective Barrier of the NPC

To further evaluate the functional importance of CPR5-gated NPC cargo transport to ETI/PCD activation and to investigate the gating mechanism, we crossed *cpr5* with stress-related karyopherin mutants as well as transport-related nucleoporin mutants (Figure S4C). We found that a partial loss-of-function mutant of Nup88, which associates with the NPC cytoplasmic filaments, could largely rescue the *cpr5* phenotypes, including the stunted growth, spontaneous PCD and elevated defense gene expression (Figures 4C and 4D). This mutant has previously been found to block nuclear accumulation of multiple defense-related proteins (Cheng et al., 2009), and its suppressor activity on *cpr5* suggests that NPC-mediated nuclear transport of immune cargos is required for CPR5-gated ETI/PCD activation. In contrast to *nup88*, crossing *cpr5* with mutants of FG nucleoporin *Nup54*, *Nup58* and *Nup136* exacerbated the *cpr5* phenotype (Figure 4E). More importantly, *Nup54* and *Nup136* display a specific inhibitory role in ETI, as their mutants were found to enhance ETI, but not basal immunity (Figure 4F). These evidence suggest that CPR5 may modulate the properties of the NPC selective barrier as a mechanism to regulate ETI. Indeed, it has been shown that loss of yeast IRC nucleoporins relaxes the NPC permeability barrier due to inappropriate anchoring of FG nucleoporins (Shulga et al., 2000). Given that CPR5 directly interacts with Nup93 (Figure 2D-2F), the molecular anchor of FG nucleoporins (Chug et al., 2015), we propose that loss-of-CPR5 activates ETI partly by perturbing the structural arrangement of FG meshwork to compromise its inhibitory role in immune signaling cargo transport.

Homomeric Interaction of CPR5 in the NPC Is Required to Inhibit ETI/PCD

Since previous genetic data clearly showed that CPR5 is a negative regulator of ETI/PCD (Boch, 1998; Wang et al., 2014), we hypothesize that its repression must be alleviated upon ETI activation. To test this, we first examined, but ruled out a significant reduction in *CPR5* transcription or translation during ETI triggered by the bacterial pathogen *Pseudomonas syringae* pv. *maculicola* (*Psm*) carrying the effector AvrRpt2 (Figure S5A–S5C). Based on the knowledge that homo- and hetero-oligomerization of nucleoporins is crucial for their functions, we then tested whether CPR5 activity is regulated through homo-oligomerization. We performed BiFC assay in *35S:n/c-YFP-CPR5* transgenic plants coexpressing n-YFP-CPR5 and c-YFP-CPR5 and found that CPR5 indeed formed a homomeric complex in the NE (Figure 5A, left). In a transient assay, the BiFC signal was also observed in the so-called Z-membranes (Figure 5A, right), which are artificial organelles formed when integral membrane proteins oligomerize through their extra-luminal domains (Gong et al., 1996). Since Z-membranes were only observed when n/cYFP were fused to the N-terminus of CPR5, we hypothesized that the CPR5 N-terminal domain is extra-luminal and mediates the homomeric interaction (Figure 5B). Indeed, *in vitro* pull-down assays mapped the homomeric interaction domain to the first two thirds of the CPR5-N (1–274 aa), with the middle region (N2) being essential (Figures 5C-5E and S5D). Notably, a known loss-of-function mutation (G120D, *old1-3*) resides in the CPR5 N2 region (Jing et al., 2007). We found that the G120D mutation significantly compromised CPR5 homomeric interaction (Figures 5F and S5E). Furthermore, at similar protein levels, the monomeric G120D allele

could not complement the *cpr5-1* phenotypes as the WT CPR5 (Figure 5G). Since the G120D mutation affected neither CPR5 localization (Figure 1D) nor CPR5 heteromeric interactions with Nup155 and Nup93a (Figure 5H), it appears to specifically affect CPR5 homomeric interaction required for its function.

CPR5 Homomeric Interaction Is Specifically Disrupted upon NB-LRR Immune Receptor Activation

We next investigated how CPR5 homomeric interaction might be regulated upon NB-LRR activation. We introduced the *35S:n/c-YFP-CPR5* into *Arabidopsis* lines carrying a dex-inducible *AvrRpt2* construct in both WT and the cognate immune receptor mutant *rps2* by genetic crosses. We found a significant reduction in the BiFC signal as early as 6 hours after dex provision when the morphology of nucleus (stained by DAPI) was still intact (Figure 6A). This reduction in CPR5 homomeric interaction was dependent on both *AvrRpt2* and RPS2 (Figure 6B), but independent of CPR5 protein levels (Figure S5C). Similar results were also obtained in the coimmunoprecipitation experiment using pathogen-challenged *Arabidopsis* plants carrying the *35S:GFP-CPR5* and *35S:HA-CPR5* double transgenes (Figure 6C). A significant reduction in CPR5 homomeric interaction was observed in response to *Psm* carrying *AvrRpt2*, but not *Psm* without the effector. These results suggest that in response to effector-triggered NB-LRR activation, the CPR5 homomeric complex in the NPC is disrupted to release its inhibition on ETI activation. This hypothesis was supported by comparing the transient CPR5-interference transcriptome described in Figure 3 with time course ETI transcriptional responses mediated by RPS4 (a TIR-NB-LRR) and RPS2 (a CC-NB-LRR). We found that the majority of the genes differentially expressed upon functional interference of CPR5 (Figure 6D, red and blue ovals) overlapped with the transcriptome changes mediated by RPS4 and RPS2 (p -value < 1e-50 in both cases), and displayed concordant expression patterns with the ETI response in WT, but not in ETI-deficient *eds1* and *rps2* mutants (Figure 6D). In contrast, those genes had limited overlap with the host transcriptome changes induced by a virulent strain that activates the basal immunity and displayed a random distribution. Lastly, we showed that overexpression of the monomeric mutant form of CPR5 (G120D) resulted in a *cpr5*-like phenotype in WT plants (Figure 6E), suggesting that disruption of CPR5 homomeric interaction is sufficient to activate ETI/PCD downstream of NB-LRR activation.

Disruption of CPR5 Homomeric Complex Coordinates ETI Signaling by Cell Cycle Regulators

Our previous study showed that physical association of CPR5 with the CKI, SIM (SIAMESE), is diminished upon *Psm/AvrRpt2* challenge, resulting in activation of a non-canonical pathway involving cell-cycle regulators that contributes to ETI and PCD (Wang et al., 2014). To test whether the interaction between CPR5 and CKIs is regulated by the homomeric interaction of CPR5, we performed an *in vitro* pull-down assay to examine the affinity of SIM to WT CPR5 and the monomeric G120D mutant. We found that the G120D mutation diminished the protein's affinity to SIM (Figures 6F and S6A). This result suggests that the homomeric CPR5-N is necessary for association with SIM, and disruption of this interaction results in the release of SIM, allowing it to engage in downstream ETI signaling. Although CKIs are required for ETI signaling, overexpressing SIM is not sufficient for

activating ETI/PCD unless the CPR5 function is compromised at the same time (Figure S6B), consistent with our hypothesis that elimination of CPR5's inhibitory activity in nuclear transport is also necessary for ETI/PCD activation.

Nucleoporins have been reported to regulate cell cycle progression through their effect on expression levels of cell cycle regulators in mammals (Chakraborty et al., 2008). The direct sequestration of the cell cycle regulators in the NPC by a transmembrane nucleoporin is a surprising finding, whose significance in basic plant cell biology is currently not known. However, this association allows the NPC to play a dual role in response to ETI induction in redirecting certain cell cycle regulators for defense gene expression and permeabilizing the NPC transport activity for simultaneous activation of diverse stress-related nuclear signaling, both of which are necessary for the activation of ETI/PCD in plants (Figure 6G).

DISCUSSION

NPC-dependent nuclear transport of immune receptors, signal transducers, and transcription factors represents a prevalent regulatory mechanism for immune activation in both plants and animals (Deslandes and Rivas, 2011; Garcia and Parker, 2009; Gilmore, 2006; Rivas, 2012). To promote nuclear translocation, protein cargos usually undergo changes in affinity to nuclear transport receptors or piggybacks on molecules with mechanisms for nuclear translocation (Wirthmueller et al., 2013). However, whether the NPC itself has a direct role in immune signaling or undergoes any specific structural change to support these immune-activated transport events was previously unknown. Our study revealed that rather than a passive conduit, the NPC is both a signaling platform and a dynamic regulator of nucleocytoplasmic cargo transport. This dual function of the NPC is directed by CPR5 and plays a necessary and sufficient role for ETI/PCD induction.

CPR5 Is a Transmembrane Nucleoporin that Inhibits ETI through Modulating Selective Transport of the NPC

Multiple *cpr5* loss-of-function mutants have been reported to confer spontaneous cell death and NB-LRR-independent resistance to pathogens carrying virulence effectors (Boch, 1998; Bowling et al., 1997), yet a direct inhibitory role for CPR5 in ETI has only recently been demonstrated with overexpression of the wild-type CPR5 showing inhibition on effector-triggered PCD and resistance (Wang et al., 2014). Here we demonstrate that CPR5 is a *bona fide* nucleoporin based on its NPC localization as well as physical and genetic interaction with the NPC core scaffold (Figures 1 and 2).

Cellular, genetic and genomic analyses showed that CPR5 inhibits ETI/PCD by constraining nuclear accumulation of a diverse array of signaling cargos (Figures 3 and 4). The enhanced defense observed in *cpr5* is the opposite of the compromised basal and ETI resistance reported for the NPC scaffold nucleoporin mutants, which are defective in bulk mRNA export (Du et al., 2016; Wiermer et al., 2012; Zhang and Li, 2005). CPR5 appears to regulate nuclear transport of signaling cargos by affecting the selective barrier composed of FG proteins, because it is physically connected with the FG protein anchor Nup93 (Figure 2D-2F) and mutants of three individual FG proteins *Nup54*, *Nup58* and *Nup136* each exacerbated the *cpr5* phenotype (Figure 4E). Importantly, mutating the FG proteins Nup54

and Nup136 alone led to enhancement of ETI, but not basal resistance (Figure 4F), suggesting that these FG proteins specifically inhibit ETI.

Disruption of CPR5 Homomeric Interaction Is an Induction Mechanism of ETI

CPR5 normally inhibits ETI at the NPC as a homomeric complex formed via its N-terminal extra-luminal domain (Figure 5). This inhibition is specifically “turned off” when CPR5 homomers are disrupted upon activation of an NB-LRR receptor RPS2 (Figures 6A-6C). Therefore, this conformational change of CPR5 in the NPC is a signaling event downstream of NB-LRRs. Moreover, this event appears to be sufficient for ETI/PCD activation as overexpression of either a N-terminus-truncated CPR5 or the G120D mutant compromised in oligomer formation resulted in the *cpr5* phenotype in the WT background (Figure S3 and Figure 6E).

Disrupting the CPR5 oligomer significantly reduces its affinity to CKIs (Figure 6F), which provides a mechanistic explanation for our previous observation that CKIs are released from CPR5 for ETI induction (Wang et al., 2014). However, ectopic expression of CKIs alone is not sufficient for mounting ETI/PCD (Figure S6B), consistent with our genetic data indicating that NPC-gated cargo transport is also necessary. Therefore, disruption of CPR5 oligomerization coordinates the two NPC actions that are collaboratively required for ETI/PCD induction.

CPR5-Mediated CKI Release and NPC Permeabilization Is a Convergent Induction Mechanism by both CC-NB-LRR and TIR-NB-LRR

We propose that during ETI, in addition to activation of distinct receptors and their signaling complexes, a common signal is generated and transduced to the NPC, leading to a disruption of CPR5 oligomer. The resulting activation of the noncanonical CKI-Rb-E2F signaling module together with the influx of nuclear signaling cargos through the NPC leads to transcriptomic changes bearing signatures of diverse hormone and stress responses (Figure 3 and 4), which overlap significantly with those induced by both a CC-NB-LRR (RPS2) and a TIR-NB-LRR (RPS4) (Figure 6D). These CPR5-regulated and NPC-gated cellular responses were barely observed in basal immunity (Figure 6D), suggesting that ETI is more than a quantitative ramping-up of basal immunity even though the two defense mechanisms have some overlap in signaling networks (Tao et al., 2003; Tsuda et al., 2009). Our study suggests that the NPC contributes a specific regulatory mechanism for simultaneous activation of diverse stress responses, which ultimately lead to the extreme outcome of ETI, i.e., PCD.

It is tempting to speculate that the NB-LRR-triggered NPC alterations in plants bear certain similarity to cellular changes associated with two distinct types of PCD in animals, apoptosis and pyroptosis. Activation of both types of PCD involves specialized mechanisms for membrane permeabilization to release pro-death factors. Activation of apoptosis requires formation of permeability transition pore (PTP) on mitochondrial membranes in order to release cytochrome c and other proteins for caspase-9 activation (Tait and Green, 2010), whereas activation of pyroptosis requires cleaved Gasdermin D to form pores on the plasma membrane to promote cell lysis and release of IL-1 β (Ding et al., 2016). Our study showed that during ETI induction, the selective barrier of the NPC becomes more permeable through

the conformational change of CPR5 to simultaneously activate diverse nuclear signaling events required for the activation of ETI and the execution of PCD in plants.

METHODS AND RESOURCES

KEY RESOURCES TABLE

REAGENT or RESOURCE	SOURCE	IDENTIFIER
Antibodies		
Mouse monoclonal anti-GFP (JL-8, for western blot)	Clontech	Cat. #632381; RRID:AB_2313808
Rabbit polyclonal anti-GFP (for immuno-EM)	Santa Cruz	Cat. #sc-8334; RRID:AB_641123
Mouse monoclonal anti-HA (16B12)	Biolegend	Cat. #901502; RRID:AB_2565007
Alpaca anti-GFP coupled to agarose beads	Chromotek	Cat. #GFP-Trap®_A
Pierce® Anti-HA Agarose	ThermoFisher	Cat. #26181; RRID:AB_2537081
Chemicals, Peptides, and Recombinant Proteins		
Dexamethasone	Sigma-Aldrich	Cat. #D1756-25MG; CAS: 50-02-2
DAPI	Sigma-Aldrich	Cat. #D9542-5MG; CAS: 28718-90-3
LR Clonase® II Plus enzyme	ThermoFisher	Cat. #12538120
Protease inhibitor cocktail	Sigma-Aldrich	Cat. #P9599-5ML; EC: 200-664-3
TRIzol Reagent	ThermoFisher	Cat. #15596026
Critical Commercial Assays		
QuikChange II site-directed mutagenesis kit	Agilent	Cat. #200524
Wheat germ <i>in vitro</i> translation system	BioSieg	N/A
SuperScript® III First-Strand Synthesis System	ThermoFisher	Cat. #18080050
FastStart Universal SYBR Green Master Kit	Roche	Cat. # 04913850001
Deposited Data		
Microarray raw and analyzed data	This paper	GEO: GSE72742, GSE72743
Experimental Models: Cell Lines		
Experimental Models: Organisms/Strains		
Arabidopsis: 35S::GFP-CPR5	Wang et al., 2014	N/A
Arabidopsis: 35S::YFP-CPR5/G120D	This paper	N/A
Arabidopsis: 35S::Dex::YFP-CPR5-C	This paper	N/A
Arabidopsis: 35S::(nYFP-CPR5+cYFP-CPR5)	This paper	N/A
Arabidopsis: 35S::(GFP-CPR5+3HA-CPR5)	This paper	N/A
Arabidopsis: GFP-WIP1	The Meier Laboratory	N/A
Arabidopsis: Nup155-YFP	This paper	N/A
Arabidopsis: MOS7-GFP	Cheng et al., 2009	N/A

REAGENT or RESOURCE	SOURCE	IDENTIFIER
<i>nup88 (mos7-1)</i> , <i>nup96 (mos3-1)</i> , <i>importin-α3 (mos6-2)</i>	The Li Laboratory, Cheng et al., 2009; Zhang and Li, 2005; Palma et al., 2005	N/A
All other nucleoporin and transport receptor mutants Used in this study, see Table S2	Arabidopsis Biological Resource Center	see Table S2 for Salk line ID
Arabidopsis: 35S::YFP-SIM	This paper	N/A
Arabidopsis: Dex::AvrRpt2	McNellis et al., 1998	N/A
Recombinant DNA		
pMDC43-GFP-CPR5	Wang et al., 2014	N/A
pEG100-YFP-CPR5 (WT and mutant constructs)	This paper	N/A
pEG100-n/cYFP-CPR5	This paper	N/A
pEG100-Nups-YFP/cYFP	This paper	N/A
pBAV154/pEG100-YFP-CPR5-C	This paper	N/A
pEG100-NPR1/JAZ1/ABI5-mCherry	This paper	N/A
pEG100-mCherry-WIT1	This paper	N/A
Sequence-Based Reagents		
Primers used in this study, see Table S3	This paper	N/A
Software and Algorithms		
Mascot (v2.5.0)	Matrix Science	N/A
Scaffold (v4.4.1.1)	Proteome Software, Inc.	N/A
R (v3.0.1)	N/A	N/A
GeneSpring (v13.0)	Agilent	N/A
MASTA	Reina-Pinto et al., 2010	N/A
PlantGSEA	Yi et al., 2013	http://structuralbiology.cau.edu.cn/PlantGSEA/
Athena	O'Connor et al., 2005	http://www.bioinformatics2.wsu.edu/cgi-bin/Athena/cgi/home.pl
Other		
REAGENT or RESOURCE		
Antibodies		
Mouse monoclonal anti-GFP (JL-8, for western blot)	Clontech	Cat. #632381; RRID:AB_2313808
Rabbit polyclonal anti-GFP (for immuno-EM)	Santa Cruz	Cat. #sc-8334; RRID:AB_641123
Mouse monoclonal anti-HA (16B12)	Biologend	Cat. #901502; RRID:AB_2565007
Alpaca anti-GFP coupled to agarose beads	Chromotek	Cat. #GFP-Trap@_A
Pierce® Anti-HA Agarose	ThermoFisher	Cat. #26181; RRID:AB_2537081
Chemicals, Peptides, and Recombinant Proteins		
Dexamethasone	Sigma-Aldrich	Cat. #D1756-25MG; CAS: 50-02-2

REAGENT or RESOURCE	SOURCE	IDENTIFIER
DAPI	Sigma-Aldrich	Cat. #D9542-5MG; CAS: 28718-90-3
LR Clonase® II Plus enzyme	Thermofisher	Cat. #12538120
Protease inhibitor cocktail	Sigma-Aldrich	Cat. #P9599-5ML; EC: 200-664-3
TRIzol Reagent	Thermofisher	Cat. #15596026
Critical Commercial Assays		
QuikChange II site-directed mutagenesis kit	Agilent	Cat. #200524
Wheat germ <i>in vitro</i> translation system	BioSieg	N/A
SuperScript® III First-Strand Synthesis System	Thermofisher	Cat. #18080050
FastStart Universal SYBR Green Master Kit	Roche	Cat. # 04913850001
Deposited Data		
Microarray raw and analyzed data	This paper	GEO: GSE72742, GSE72743
Experimental Models: Cell Lines		
Experimental Models: Organisms/Strains		
Arabidopsis: 35S::GFP-CPR5	Wang et al., 2014	N/A
Arabidopsis: 35S::YFP-CPR5/G120D	This paper	N/A
Arabidopsis: 35S::Dex::YFP-CPR5-C	This paper	N/A
Arabidopsis: 35S::nYFP-CPR5+cYFP-CPR5	This paper	N/A
Arabidopsis: 35S::GFP-CPR5+3HA-CPR5	This paper	N/A
Arabidopsis: GFP-WIP1	The Meier Laboratory	N/A
Arabidopsis: Nup155-YFP	This paper	N/A
Arabidopsis: MOS7-GFP	Cheng et al., 2009	N/A
<i>nup88 (mos7-1)</i> , <i>nup96 (mos3-1)</i> , <i>importin-α3 (mos6-2)</i>	The Li Laboratory, Cheng et al., 2009; Palma et al., 2005; Zhang and Li, 2005	N/A
All other nucleoporin and transport receptor mutants Used in this study, see Table S2	Arabidopsis Biological Resource Center	see Table S2 for Salk line ID
Arabidopsis: 35S::YFP-SIM	This paper	N/A
Arabidopsis: Dex::AvrRpt2	McNellis et al., 1998	N/A
Recombinant DNA		
pMDC43-GFP-CPR5	Wang et al., 2014	N/A
pEG100-YFP-CPR5 (WT and mutant constructs)	This paper	N/A
pEG100-n/cYFP-CPR5	This paper	N/A
pEG100-Nups-YFP/cYFP	This paper	N/A
pBAV154/pEG100-YFP-CPR5-C	This paper	N/A
pEG100-NPR1/JAZ1/ABI5-mCherry	This paper	N/A
pEG100-mCherry-WIT1	This paper	N/A
Sequence-Based Reagents		

REAGENT or RESOURCE	SOURCE	IDENTIFIER
Primers used in this study, see Table S3	This paper	N/A
<i>Software and Algorithms</i>		
Mascot (v2.5.0)	Matrix Science	N/A
Scaffold (v4.4.1.1)	Proteome Software, Inc.	N/A
R (v3.0.1)	N/A	N/A
GeneSpring (v13.0)	Agilent	N/A
MASTA	Reina-Pinto et al., 2010	N/A
PlantGSEA	Yi et al., 2013	http://structuralbiology.cau.edu.cn/PlantGSEA/
Athena	O'Connor et al., 2005	http://www.bioinformatics2.wsu.edu/cgi-bin/Athena/cgi/home.pl
<i>Other</i>		

CONTACT FOR REAGENT AND RESOURCE SHARING

Further information and requests for reagents may be directed to, and will be fulfilled by the corresponding author Xinnian Dong (xdong@duke.edu).

EXPERIMENTAL MODEL AND SUBJECT DETAILS

Arabidopsis

All *Arabidopsis* plants used in this study were in the Col-0 background. Wild type (WT), mutant, and transgenic *Arabidopsis* seeds were stratified at 4°C for two days and plants were grown under a 12-hrs light and 12-hrs dark cycle at 22°C. *GFP-WIP1*, *NPR1-GFP*, *Nup155-YFP* and *MOS7-GFP* were introduced into the *cpr5* mutant background through genetic crosses. Nucleoporin and transport receptor mutants used in this study were Salk T-DNA insertion lines obtained from Arabidopsis Biological Resource Center (see Table S2 for Salk line information) or *mos* mutants (Cheng et al., 2009; Palma et al., 2005; Zhang and Li, 2005) provided by Dr. Xin Li's laboratory (see Table S2). *cpr5 nup* double mutants were obtained through genetic crosses. *35S:YFP-CPR5-C* and *Dex:YFP-CPR5-C* were transformed into WT background for functional interference of CPR5 and subsequently crossed to the *cpr5* mutant as controls to test the specificity of the interference effect. To obtain *35S:GFP-CPR5/HA-CPR5* double transgenic line, a previously reported *35S:GFP-CPR5* line (Wang et al., 2014) was transformed with *35S:HA-CPR5*. T3 progeny homozygous for both transgenes were used for experiments. Isogenic *35S:n/c YFP-CPR5* line and *Dex:AvrRpt2* line (McNellis et al., 1998) were generated in WT and *rps2* backgrounds, respectively. The *35S:n/c YFP-CPR5/Dex:AvrRpt2* double transgenic lines were obtained by genetic crosses.

METHOD DETAILS

Plasmid Construction

All point mutations of *CPR5* were generated using the QuikChange II site-directed mutagenesis kit (Agilent). The full-length cDNA of *CPR5*, *WIT1*, *SIM* and all *CPR5* mutant constructs including the single-site mutations and truncations were cloned into pBSDONR p4r-p2, a multisite gateway donor vector for N-terminal tagging (Gu and Innes, 2011). The full-length cDNA of *Nup136*, *Nup93a*, *Nup35*, *NPR1*, *JAZ1*, *ABI5* and the genomic DNA fragments (from start codon to stop codon) of *Nup155*, *Nup96*, *Nup88*, *Nup85*, *Nup62*, *Nup58*, *Nup54*, *HOS1* were cloned into pBSDONR p1-p4, a multisite gateway donor vector for C-terminal tagging. Those clones were then paired with fluorescent tags, n/c-YFP (for BiFC) or 3xHA tag cloned in pBSDONR p1-p4 or pBSDONR p4r-p2, to generate fusion constructs in pEG100 or pBAV154 destination vector by LR reaction (LR clonase II plus, Thermofisher) for constitutive or dexamethasone inducible expression, respectively. To generate *35S:n/cYFP-CPR5* construct used in transgenic line, *nYFP-CPR5* was first cloned in pGWB414 by LR reaction and a fragment including the promoter, the fusion construct and the terminator was amplified, cut by AseI and ligated into pEG100, which already contains an independent expression cassette for the *cYFP-CPR5* fusion. All constructs were verified by sequencing before use.

Transient Expression Assays

Agrobacterium-mediated transient expression in *N. benthamiana* and transformation of *Arabidopsis* protoplasts were performed as described (Gu and Innes, 2011).

Confocal Laser Scanning Microscopy

Intracellular fluorescence was observed using a Leica SP8 upright confocal microscope with high sensitivity hybrid detectors. Intracellular membrane organelle markers used were described previously (Brkljacic et al., 2009; Gu and Innes, 2011, 2012; Nelson et al., 2007). Three-dimensional image reconstruction and co-localization statistics were carried out using IMARIS 8.0 (Bitplane). FRAP experiment was performed using Leica SP8 FRAP Wizard. Fluorescence intensity was normalized to the average expression level defined by random sampling before photobleaching. Recovery curves were plotted with 50 frames (1 frame/sec) recorded after photobleaching.

Immunoelectron Microscopy and Electron Tomography

Root tip samples were dissected from *Arabidopsis* seedlings expressing GFP-CPR5 and cryofixed by an HPM100 (Leica Microsystems). The frozen specimens were freeze-substituted at -80°C and embedded in HM20 resin (Electron Microscopy Sciences) at -45°C . After polymerization at -45°C , the root tip samples were sectioned and immunolabeled with a GFP antibody (Santa Cruz) as described previously (Kang, 2010).

Co-Immunoprecipitation

All tagged proteins for *in vitro* pull-down assays were synthesized using a wheat germ-based transcription/translation system (BioSieg). Synthesized proteins were mixed and incubated

with GFP-TrapA (Chromo Tek) or Pierce anti-HA agarose beads (ThermoFisher) overnight at 4°C in the pull-down buffer (50 mM Tris, pH 7.5, 150 mM NaCl, 0.1% Triton X-100, 0.2% Nonidet P-40, plant protease inhibitor cocktail (Sigma) and 40 µM MG115). Following immunoprecipitation (IP), beads were precipitated and washed five times with the pull-down buffer before eluted with the SDS sample buffer. For *in vivo* co-immunoprecipitation, leaf tissues of four-week-old transgenic plants were collected. Total protein was extracted using IP buffer with high concentration of detergents to completely solubilize membrane protein (50 mM Tris, pH7.5, 150 mM NaCl, 0.5% Triton X-100, 0.5% Nonidet P-40, 0.25% Na-deoxycholate, plant protease inhibitor cocktail, and 40 mM MG115) followed by immunoprecipitation with GFP-TrapA beads overnight at 4°C. After IP, beads were washed five times with the IP buffer. Samples were boiled with loading buffer for 10 min before separated by SDS-PAGE.

LC-MS/MS and Data Analysis

A total of 5 g leaf tissues from four-week-old transgenic plants were collected. Total protein was extracted with IP buffer (50 mM Tris, pH7.5, 150 mM NaCl, 0.5% Triton X-100, 0.5% Nonidet P-40, plant protease inhibitor cocktail, and 40 mM MG115) and immunoprecipitated with GFP-TrapA beads overnight at 4°C. After IP, samples were washed five times with the IP buffer and three times with 50 mM NH₄HCO₃ before on-bead trypsin digestion. Following immunoprecipitation, on-bead trypsin digestion, peptide lyophilization and LC-MS/MS were performed by the Duke Proteomics Core Facility. MS/MS samples were analyzed using Mascot (Matrix Science, London, UK; version 2.5.0) and searched with a fragment ion mass tolerance of 0.020 Da and a parent ion tolerance of 5.0 PPM. Scaffold (version 4.4.1.1, Proteome Software Inc., Portland, OR) was used to validate MS/MS based peptide and protein identifications. Peptide/protein identifications were accepted if they could be established at greater than 95% probability by the Peptide/Protein Prophet algorithm, which yielded a false-discovery rate of 0.1% and 0.5% on the peptide and protein match level, respectively. Data from *35S:GFP* samples ran in parallel were used as controls for a statistical model-based selection of CPR5-specific interactors. A total of 41 candidates were identified and this list was shortened to 28 by further excluding proteins that are abundant in chloroplasts and mitochondria. Predicted interactions between CPR5 interactors were based on an interolog method (Geisler-Lee et al., 2007).

Quantitative PCR

Arabidopsis RNA was extracted using TRIzol Reagent (ThermoFisher), and cDNA was synthesized using the SuperScript III cDNA Synthesis (ThermoFisher). Quantitative PCR (qPCR) was performed using FastStart Universal SYBR Green Master Kit (Roche) in Mastercycler ep realplex (Eppendorf).

Microarray Procedure and Data Analysis

For *RPS2*-dependent ETI response, four-week-old WT and *rps2* mutant plants were inoculated with *PsmIAvrRpt2*. At 0, 6 and 10 hrs post inoculation, leaf tissues were collected for RNA preparation and microarray. The resulting data set was deposited to Gene Expression Omnibus (GEO: GSE72742). For transient interference of the CPR5 function, four-week-old WT and T3 homozygous *Dex:YFP-CPR5-C* transgenic plants were sprayed

with water or 50 μ M dexamethasone (Sigma). After 24 hrs, leaf tissues were collected for RNA preparation and microarray. The resulting data set was deposited to GEO: GSE72743. RNA quality control, cDNA synthesis, aRNA purification and fragmentation, hybridization, washing and scanning of *Arabidopsis* ATH1 Genome Arrays (Affymetrix) chips were performed by the Duke Microarray Facility. For CPR5-C interference microarray, differentially expressed genes were further filtered by subtracting genes whose expression are affected by the empty vector control upon dexamethasone induction (GSE8741). The resulting gene list was provided in Table S1. The *RPS4*-dependent ETI genes, *RPS2*-dependent ETI genes and basal immunity genes were determined by microarray analysis of dataset GSE50019, GSE73742 and GSE17464, respectively. Statistical analysis and natural language processing-based network regulator discovery were performed using GeneSpring 13.0 (Agilent, 2014) and R 3.0.1 (2013). Networks were established based on published transcriptional regulatory relationships between genes and physical interactions between proteins. Comparative microarray analysis and GSEA were performed using MASTA (Reina-Pinto et al., 2010) and PlantGSEA (Yi et al., 2013), respectively. *Cis*-element enrichment was analyzed using total differentially expressed genes with Athena (O'Connor et al., 2005).

Bacterial Growth Assay

Infection of *Arabidopsis* plants with *Psm* ES4326 (with or without *AvrRpt2*) was performed as described previously (Wang et al., 2014). Bacterial suspension of $OD_{600nm} = 0.001$ was infiltrated into 2 leaves per plant and 12 plants per genotype. Each experimental replication contained four leaf discs from two plants. Bacterial growth was quantified at 0 and 3 days post infiltration.

Primers

All primers used in this study were listed in Table S3.

QUANTIFICATION AND STATISTICAL ANALYSIS

The nuclear circularity index is defined as $4\pi A/P^2$, where A and P are the cross-sectional area and perimeter of the nucleus, respectively. A and P were measured for each nucleus using Fiji. Bacterial growth was reported as the number of colony forming units (cfu), which was subject to log transformation. For fluorescence quantification using Fiji, the fluorescence intensity was calculated using Integrated Density – (Area of selected cell \times Mean fluorescence of background). Nuclear circularity, log(cfu) and fluorescence intensity data were assumed to follow normal distributions and were subjected to two-tailed Student's *t*-test or ANOVA, where appropriate. Statistical tests were performed in GraphPad Prism 6. Statistical parameters including the exact value of n, the definition of center, dispersion and precision measures (mean \pm SDM) and statistical significance can be found in the Figure Legends. In Figures, asterisks denote statistical significance test (*, $p < 0.05$; **, $p < 0.01$; ***, $p < 0.001$; ****, $p < 0.0001$) as compared to untreated controls, unless otherwise specified by lines connecting the compared pieces of data. For LC-MS/MS analysis, exclusive spectrum count data were assumed to follow a Gamma-Poisson distribution. After normalized by size factors, negative binomial regression models were built with the

normalized data using DESeq2 package in R, which provided the cutoff to select for CPR5-specific interactors (p -value < 0.05 , fold change > 2.5 , CPR5 vs GFP). For microarray analysis, array data were summarized using the Robust Multiarray Average method using GeneSpring and the normal distribution of the expression data were verified using EMA package in R. CPR5-C-induced differentially expressed genes were selected using 2-way ANOVA model (p -value < 0.01 , fold change > 2 , dex vs water); the *RPS4*-dependent ETI genes were determined by 2-way ANOVA (p -value < 0.01 , fold change > 2) using the signaling mutant *eds1* as a control (GSE50019); the *RPS2*-dependent ETI genes induced by *Psm/AvrRpt2* was determined by 2-way ANOVA (p -value < 0.01 , fold change > 2) using the immune receptor mutant *rps2* as a control (GSE72742); the basal immunity induced by *Pst* DC3000 was determined by Moderated t -test (p -value < 0.05 and fold change > 2 , GSE17464).

DATA AND SOFTWARE AVAILABILITY

Data Resources

Raw data files for the microarray analysis have been deposited in the NCBI Gene Expression Omnibus under accession number GSE72742 and GSE72743.

Supplementary Material

Refer to Web version on PubMed Central for supplementary material.

Acknowledgments

The authors thank Dr. Roger Innes for providing membrane organelle markers and Dr. Iris Meier for sharing the *35S:GFP-WIP1* and *35S:RanGAP1-GFP* transgenic lines. We also thank Drs. Iris Meier, Paul Zwack and John Withers for critical reading of the manuscript. This work was supported by the Howard Hughes Medical Institute and the Gordon and Betty Moore Foundation (through grant GBMF3032) and by grants from the National Institutes of Health (NIH) (R01-GM069594) to X.D., the National Natural Science Foundation of China (Grant No. 31571254) to S.W., and Rural Development Administration, Republic of Korea (Project No. 10953092015) and Research Grants Council of Hong Kong (AoE/M-05/12, C4011-14R) to B.K..

REFERENCES

- Alber F, Dokudovskaya S, Veenhoff LM, Zhang W, Kipper J, Devos D, Suprpto A, Karni-Schmidt O, Williams R, Chait BT, Sali A, Rout MP. The molecular architecture of the nuclear pore complex. *Nature*. 2007; 450:695–701. [PubMed: 18046406]
- Boch J, Verbsky ML, Robertson TL, Larkin JC, Kunkel BN. Analysis of Resistance Gene-Mediated Defense Responses in Arabidopsis thaliana Plants Carrying a Mutation in CPR5. *Mol. Plant Microbe Interact*. 1998; 11:1196–1206.
- Bowling SA, Clarke JD, Liu Y, Klessig DF, Dong X. The *cpr5* mutant of Arabidopsis expresses both NPR1-dependent and NPR1-independent resistance. *Plant Cell*. 1997; 9:1573–1584. [PubMed: 9338960]
- Brkljacic J, Zhao Q, Meier I. WPP-domain proteins mimic the activity of the HSC70-1 chaperone in preventing mistargeting of RanGAP1-anchoring protein WIT1. *Plant Physiol*. 2009; 151:142–154. [PubMed: 19617588]
- Chakraborty P, Wang Y, Wei JH, van Deursen J, Yu H, Malureanu L, Dasso M, Forbes DJ, Levy DE, Seemann J, Fontoura BM. Nucleoporin levels regulate cell cycle progression and phase-specific gene expression. *Dev. Cell*. 2008; 15:657–667. [PubMed: 19000832]

- Cheng YT, Germain H, Wiermer M, Bi D, Xu F, Garcia AV, Wirthmueller L, Despres C, Parker JE, Zhang Y, Li X. Nuclear pore complex component MOS7/Nup88 is required for innate immunity and nuclear accumulation of defense regulators in Arabidopsis. *Plant Cell*. 2009; 21:2503–2516. [PubMed: 19700630]
- Chug H, Trakhanov S, Hulsmann BB, Pleiner T, Gorlich D. Crystal structure of the metazoan Nup62*Nup58*Nup54 nucleoporin complex. *Science*. 2015
- Deslandes L, Rivas S. The plant cell nucleus: a true arena for the fight between plants and pathogens. *Plant Signal. Behav.* 2011; 6:42–48. [PubMed: 21258210]
- Ding J, Wang K, Liu W, She Y, Sun Q, Shi J, Sun H, Wang DC, Shao F. Pore-forming activity and structural autoinhibition of the gasdermin family. *Nature*. 2016; 535:111–116. [PubMed: 27281216]
- Dong CH, Hu X, Tang W, Zheng X, Kim YS, Lee BH, Zhu JK. A putative Arabidopsis nucleoporin, AtNUP160, is critical for RNA export and required for plant tolerance to cold stress. *Mol. Cell Biol.* 2006; 26:9533–9543. [PubMed: 17030626]
- Du J, Gao Y, Zhan Y, Zhang S, Wu Y, Xiao Y, Zou B, He K, Gou X, Li G, Lin H, Li J. Nucleocytoplasmic trafficking is essential for BAK1- and BKK1-mediated cell-death control. *Plant J.* 2016; 85:520–531. [PubMed: 26775605]
- Elmore JM, Lin ZJ, Coaker G. Plant NB-LRR signaling: upstreams and downstreams. *Curr. Opin. Plant Biol.* 2011; 14:365–371. [PubMed: 21459033]
- Garcia AV, Parker JE. Heaven's Gate: nuclear accessibility and activities of plant immune regulators. *Trends Plant Sci.* 2009; 14:479–487. [PubMed: 19716748]
- Geisler-Lee J, O'Toole N, Ammar R, Provart NJ, Millar AH, Geisler M. A predicted interactome for Arabidopsis. *Plant Physiol.* 2007; 145:317–329. [PubMed: 17675552]
- Gilmore TD. Introduction to NF-kappaB: players, pathways, perspectives. *Oncogene*. 2006; 25:6680–6684. [PubMed: 17072321]
- Gong FC, Giddings TH, Meehl JB, Staehelin LA, Galbraith DW. Z-membranes: artificial organelles for overexpressing recombinant integral membrane proteins. *Proc. Natl. Acad. Sci. U S A.* 1996; 93:2219–2223. [PubMed: 8700911]
- Gu Y, Innes RW. The KEEP ON GOING protein of Arabidopsis recruits the ENHANCED DISEASE RESISTANCE1 protein to trans-Golgi network/early endosome vesicles. *Plant Physiol.* 2011; 155:1827–1838. [PubMed: 21343429]
- Gu Y, Innes RW. The KEEP ON GOING protein of Arabidopsis regulates intracellular protein trafficking and is degraded during fungal infection. *Plant Cell*. 2012; 24:4717–4730. [PubMed: 23192225]
- Jevtic P, Edens LJ, Vukovic LD, Levy DL. Sizing and shaping the nucleus: mechanisms and significance. *Curr. Opin. Cell Biol.* 2014; 28:16–27. [PubMed: 24503411]
- Jing HC, Anderson L, Sturre MJ, Hille J, Dijkwel PP. Arabidopsis CPR5 is a senescence-regulatory gene with pleiotropic functions as predicted by the evolutionary theory of senescence. *J. Exp. Bot.* 2007; 58:3885–3894. [PubMed: 18033818]
- Jones JD, Dangl JL. The plant immune system. *Nature*. 2006; 444:323–329. [PubMed: 17108957]
- Kang BH. Electron microscopy and high-pressure freezing of Arabidopsis. *Methods Cell Biol.* 2010; 96:259–283. [PubMed: 20869527]
- Lee H, Xiong L, Gong Z, Ishitani M, Stevenson B, Zhu JK. The Arabidopsis HOS1 gene negatively regulates cold signal transduction and encodes a RING finger protein that displays cold-regulated nucleo-cytoplasmic partitioning. *Genes. Dev.* 2001; 15:912–924. [PubMed: 11297514]
- Lee Y, Lee HS, Lee JS, Kim SK, Kim SH. Hormone- and light-regulated nucleocytoplasmic transport in plants: current status. *J. Exp. Bot.* 2008; 59:3229–3245. [PubMed: 18678754]
- Mans BJ, Anantharaman V, Aravind L, Koonin EV. Comparative genomics, evolution and origins of the nuclear envelope and nuclear pore complex. *Cell Cycle*. 2004; 3:1612–1637. [PubMed: 15611647]
- McNellis TW, Mudgett MB, Li K, Aoyama T, Horvath D, Chua NH, Staskawicz BJ. Glucocorticoid-inducible expression of a bacterial avirulence gene in transgenic Arabidopsis induces hypersensitive cell death. *Plant J.* 1998; 14:247–257. [PubMed: 9628020]
- Nelson BK, Cai X, Nebenfuhr A. A multicolored set of in vivo organelle markers for co-localization studies in Arabidopsis and other plants. *Plant J.* 2007; 51:1126–1136. [PubMed: 17666025]

- O'Connor TR, Dyreson C, Wyrick JJ. Athena: a resource for rapid visualization and systematic analysis of Arabidopsis promoter sequences. *Bioinformatics*. 2005; 21:4411–4413. [PubMed: 16223790]
- Palma K, Zhang Y, Li X. An importin alpha homolog, MOS6, plays an important role in plant innate immunity. *Curr. Biol*. 2005; 15:1129–1135. [PubMed: 15964279]
- Parry G. Components of the Arabidopsis nuclear pore complex play multiple diverse roles in control of plant growth. *J. Exp. Bot*. 2014; 65:6057–6067. [PubMed: 25165147]
- Parry G, Ward S, Cernac A, Dharmasiri S, Estelle M. The Arabidopsis SUPPRESSOR OF AUXIN RESISTANCE proteins are nucleoporins with an important role in hormone signaling and development. *Plant Cell*. 2006; 18:1590–1603. [PubMed: 16751346]
- Reina-Pinto JJ, Voisin D, Teodor R, Yephremov A. Probing differentially expressed genes against a microarray database for in silico suppressor/enhancer and inhibitor/activator screens. *Plant J*. 2010; 61:166–175. [PubMed: 19811619]
- Rivas S. Nuclear dynamics during plant innate immunity. *Plant Physiol*. 2012; 158:87–94. [PubMed: 21951465]
- Shulga N, Mosammaparast N, Wozniak R, Goldfarb DS. Yeast nucleoporins involved in passive nuclear envelope permeability. *J. Cell Biol*. 2000; 149:1027–1038. [PubMed: 10831607]
- Strambio-De-Castillia C, Niepel M, Rout MP. The nuclear pore complex: bridging nuclear transport and gene regulation. *Nat. Rev. Mol. Cell Biol*. 2010; 11:490–501. [PubMed: 20571586]
- Stuart LM, Paquette N, Boyer L. Effector-triggered versus pattern-triggered immunity: how animals sense pathogens. *Nat. Rev. Immunol*. 2013; 13:199–206. [PubMed: 23411798]
- Tait SW, Green DR. Mitochondria and cell death: outer membrane permeabilization and beyond. *Nat. Rev. Mol. Cell Biol*. 2010; 11:621–632. [PubMed: 20683470]
- Tamura K, Fukao Y, Iwamoto M, Haraguchi T, Hara-Nishimura I. Identification and characterization of nuclear pore complex components in Arabidopsis thaliana. *Plant Cell*. 2010; 22:4084–4097. [PubMed: 21189294]
- Tao Y, Xie Z, Chen W, Glazebrook J, Chang HS, Han B, Zhu T, Zou G, Katagiri F. Quantitative nature of Arabidopsis responses during compatible and incompatible interactions with the bacterial pathogen *Pseudomonas syringae*. *Plant Cell*. 2003; 15:317–330. [PubMed: 12566575]
- Toyama BH, Savas JN, Park SK, Harris MS, Ingolia NT, Yates JR, Hetzer MW 3rd. Identification of long-lived proteins reveals exceptional stability of essential cellular structures. *Cell*. 2013; 154:971–982. [PubMed: 23993091]
- Tsuda K, Sato M, Stoddard T, Glazebrook J, Katagiri F. Network properties of robust immunity in plants. *PLoS Genet*. 2009; 5:e1000772. [PubMed: 20011122]
- Verslues PE, Guo Y, Dong CH, Ma W, Zhu JK. Mutation of SAD2, an importin beta-domain protein in Arabidopsis, alters abscisic acid sensitivity. *Plant J*. 2006; 47:776–787. [PubMed: 16889648]
- Wang S, Gu Y, Zebell SG, Anderson LK, Wang W, Mohan R, Dong X. A noncanonical role for the CKI-RB-E2F cell-cycle signaling pathway in plant effector-triggered immunity. *Cell Host Microbe*. 2014; 16:787–794. [PubMed: 25455564]
- Washburn MP, Wolters D, Yates JR 3rd. Large-scale analysis of the yeast proteome by multidimensional protein identification technology. *Nat. Biotechnol*. 2001; 19:242–247. [PubMed: 11231557]
- Wiermer M, Cheng YT, Imkampe J, Li M, Wang D, Lipka V, Li X. Putative members of the Arabidopsis Nup107-160 nuclear pore sub-complex contribute to pathogen defense. *Plant J*. 2012; 70:796–808. [PubMed: 22288649]
- Wirthmueller L, Roth C, Banfield MJ, Wiermer M. Hop-on hop-off: importin-alpha-guided tours to the nucleus in innate immune signaling. *Front. Plant Sci*. 2013; 4:149. [PubMed: 23734157]
- Yi X, Du Z, Su Z. PlantGSEA: a gene set enrichment analysis toolkit for plant community. *Nucleic Acids Res*. 2013; 41:W98–W103. [PubMed: 23632162]
- Yoshida S, Ito M, Nishida I, Watanabe A. Identification of a novel gene HYS1/CPR5 that has a repressive role in the induction of leaf senescence and pathogen-defence responses in Arabidopsis thaliana. *Plant J*. 2002; 29:427–437. [PubMed: 11846876]

Zhang Y, Li X. A putative nucleoporin 96 Is required for both basal defense and constitutive resistance responses mediated by suppressor of npr1-1, constitutive 1. *Plant Cell*. 2005; 17:1306–1316. [PubMed: 15772285]

Author Manuscript

Author Manuscript

Author Manuscript

Author Manuscript

In Brief

Rather than being a passive conduit, the nuclear pore complex in response to immune signals undergoes a conformational switch to reconfigure the selective barrier and promote stress responses.

Author Manuscript

Author Manuscript

Author Manuscript

Author Manuscript

Highlights

- CPR5 is a component of the nuclear pore complex (NPC)
- CPR5 regulates nuclear transport through the selective barrier of the NPC
- CPR5 homomer is disrupted upon induction of effector-triggered immunity (ETI).
- Conformational change in CPR5 leads to CKI release and NPC permeabilization for ETI.

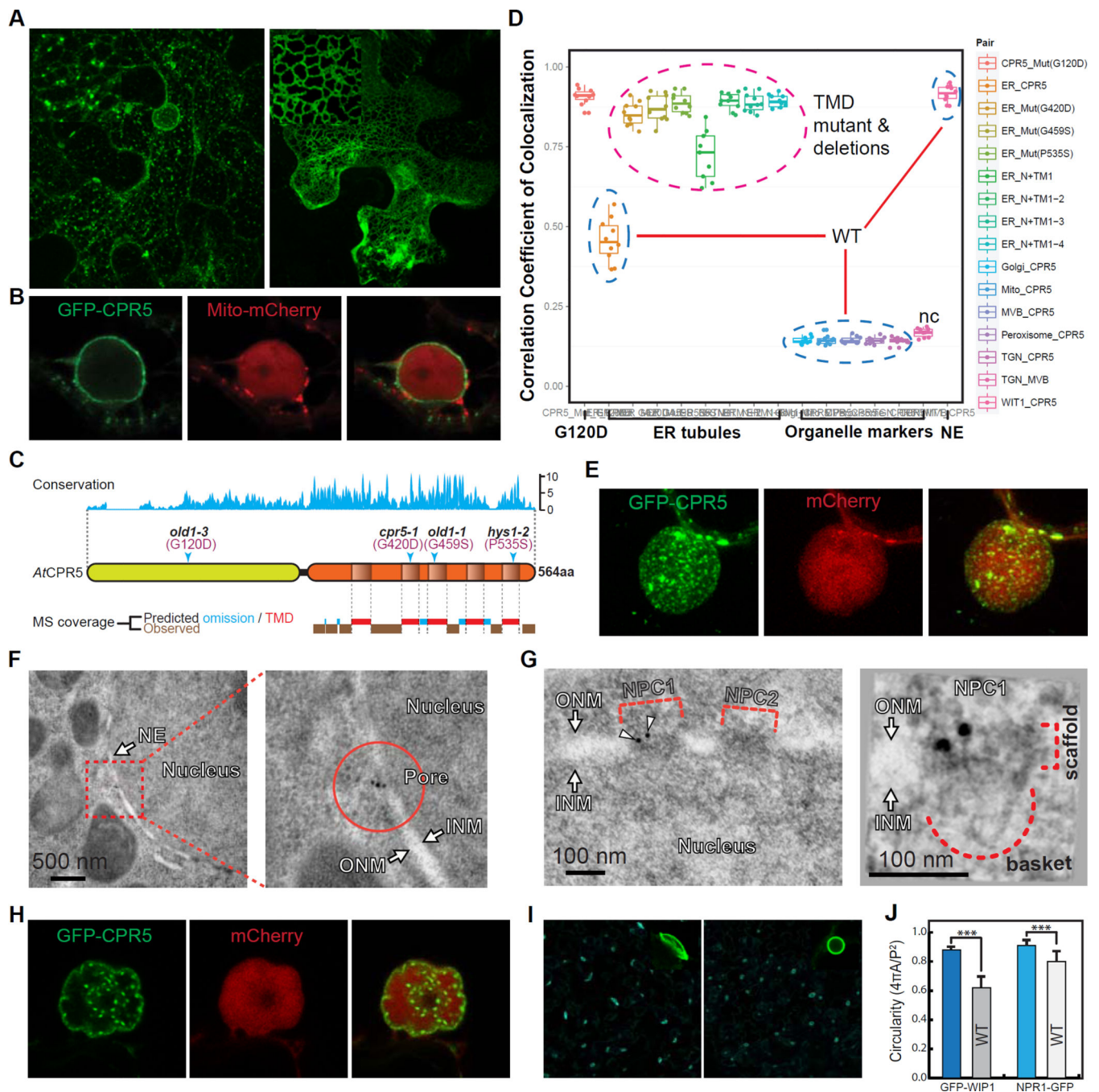


Figure 1. CPR5 Is a Transmembrane Protein Enriched in the Nuclear Pore

(A and B) Subcellular localization of GFP-tagged CPR5 when transiently expressed in *N. benthamiana*. Wild-type (WT) CPR5 (A, left), the G420D mutant (A, right), and WT CPR5 co-expressed with a mCherry-tagged marker labeling mitochondria and nucleoplasm (B) were shown. Images were obtained 24 hrs post *Agrobacterium* infiltration. (C) CPR5 contains an evolutionarily conserved transmembrane (TM) region at the carboxyl terminus. Top, amino acid conservation map derived from multiple sequence alignments of CPR5 proteins from *Micromonas pusilla*, *Chlorella variabilis*, *Physcomitrella patens*,

Sorghum bicolor, *Selaginella moellendorffii*, *Vitis vinifera*, *Populus trichocarpa*, *Ricinus communis*, *Oryza sativa*, *Zea mays* and *Arabidopsis thaliana*. Middle, schematic of AtCPR5 domain structure with transmembrane TM domains (TMDs) predicted by TMPred. Arrowheads indicate sites of loss-of-function missense mutations. Bottom, LC-MS/MS peptide coverage in the C-terminal half of AtCPR5 purified from transgenic *Arabidopsis*. Predicted omissions were calculated by PeptideMass for trypsin digestion (see Figure S1C). (D) Pearson's correlation coefficients of co-localization between CPR5 and endomembrane organelle markers. WT CPR5 (blue dashed circles) co-localized with both the nuclear envelope (NE) marker (WIT1) and ER-associated granules (see Figure S1B). CPR5 with missense mutations in the TMDs (Mut) and sequential truncations of individual TMDs (N+TM) all exclusively localized in tubular ER structures (magenta dashed circle). TGN (early endosome) and MVB (late endosome) markers were used as a negative control (nc). (E) Three-dimensional image reconstruction of the nuclear surface in a GFP-CPR5 expressing cell. The nucleoplasm is labeled by free mCherry. Arrowheads indicate large ER-associated granules close to the nuclear surface. (F and G) Immunoelectron microscopy and tomography analyses of GFP-CPR5 in root cells of transgenic *Arabidopsis*. Immunogold particles (arrowheads) labeled NPC1 but not NPC2 as antibodies detect only surface-exposed epitopes (G, left). The scaffold and nuclear basket of NPC1 were recognized together with two GFP-CPR5 specific immunogold particles in a projection of the tomographic volume (G, right). ONM/INM, outer/inner nuclear membrane. (H) Hypolobulated NE and inner nuclear speckles resulted from prolonged overexpression of GFP-CPR5 (40 hrs after *Agrobacterium* infiltration). (I and J) Nuclear morphology in WT and *cpr5* mutant plants. Epidermal cells of 5-day-old seedlings expressing the NE marker GFP-WIP1 were imaged (I). Quantification of the nuclear circularity was performed using GFP-WIP1 and NPR1-GFP as NE and nucleoplasm markers, respectively (J). Data are presented as mean \pm SDM (n = 30 cells for each marker and genotype). Asterisks indicate significance (Student's *t*-test, ****p*-value < 0.001). See also Figure S1.

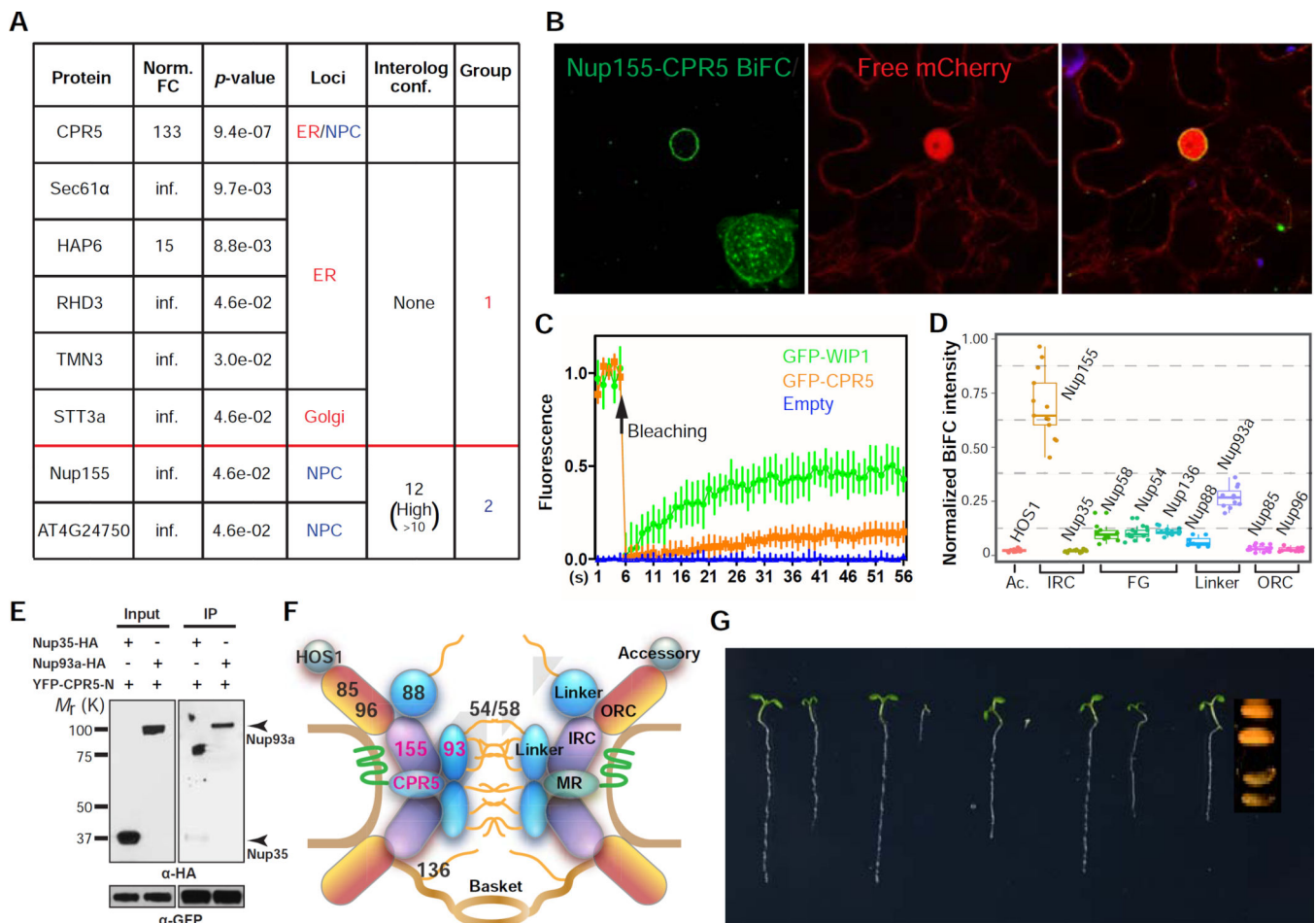


Figure 2. CPR5 Physically and Genetically Interacts with Nucleoporins as a Component of the NPC

(A) CPR5 interactors identified by protein complex purification followed by LC-MS/MS. FC, fold change of spectrum counts in YFP-CPR5 vs GFP sample. Infinite (inf.) indicates that peptide was not detected in GFP samples. Interolog conf., confidence of predicted interaction between proteins.

(B) CPR5 and Nup155 interacts in the NE. Bimolecular fluorescence complementation (BiFC) assay was performed by transiently coexpressing nYFP-CPR5 and Nup155-cYFP in *N. benthamiana*. The interaction pattern on the nuclear surface was reconstructed by Z-stack images (inset).

(C) Fluorescence Recovery After Photobleaching (FRAP) analysis of GFP-CPR5 in transgenic *Arabidopsis*. A mobile NE protein GFP-WIP1 served as a control. Data are presented as mean \pm SDM ($n = 5$ experimental replications).

(D) Interaction mapping of CPR5 with nucleoporins. BiFC was performed by transiently coexpressing nYFP-CPR5 with Nup-cYFP in *N. benthamiana*. The BiFC intensity was normalized using averaged expression levels of corresponding Nup-YFP measured in separate experiments. Ac, accessory nucleoporin; IRC, inner ring complex; FG, Phe-Gly repeat-containing nucleoporin; ORC, outer ring complex; Linker, linker nucleoporin.

(E) CPR5 interacts with the IRC-associated linker nucleoporin Nup93a. *In vitro* pulldown assay was performed using GFP-TrapA agarose beads. YFP-CPR5-N, YFP-tagged N-terminal half of CPR5.

(F) The structural modules of the nuclear pore complex (NPC) and the proposed position of CPR5 within the NPC.

(G) Genetic interaction between *cpr5* and mutants of the ORC nucleoporins. 5-day-old seedlings were shown. Since the *cpr5 nup160* double mutant did not germinate, the seed morphology of the homozygote was compared to that of a heterozygote. See also Figure S2.

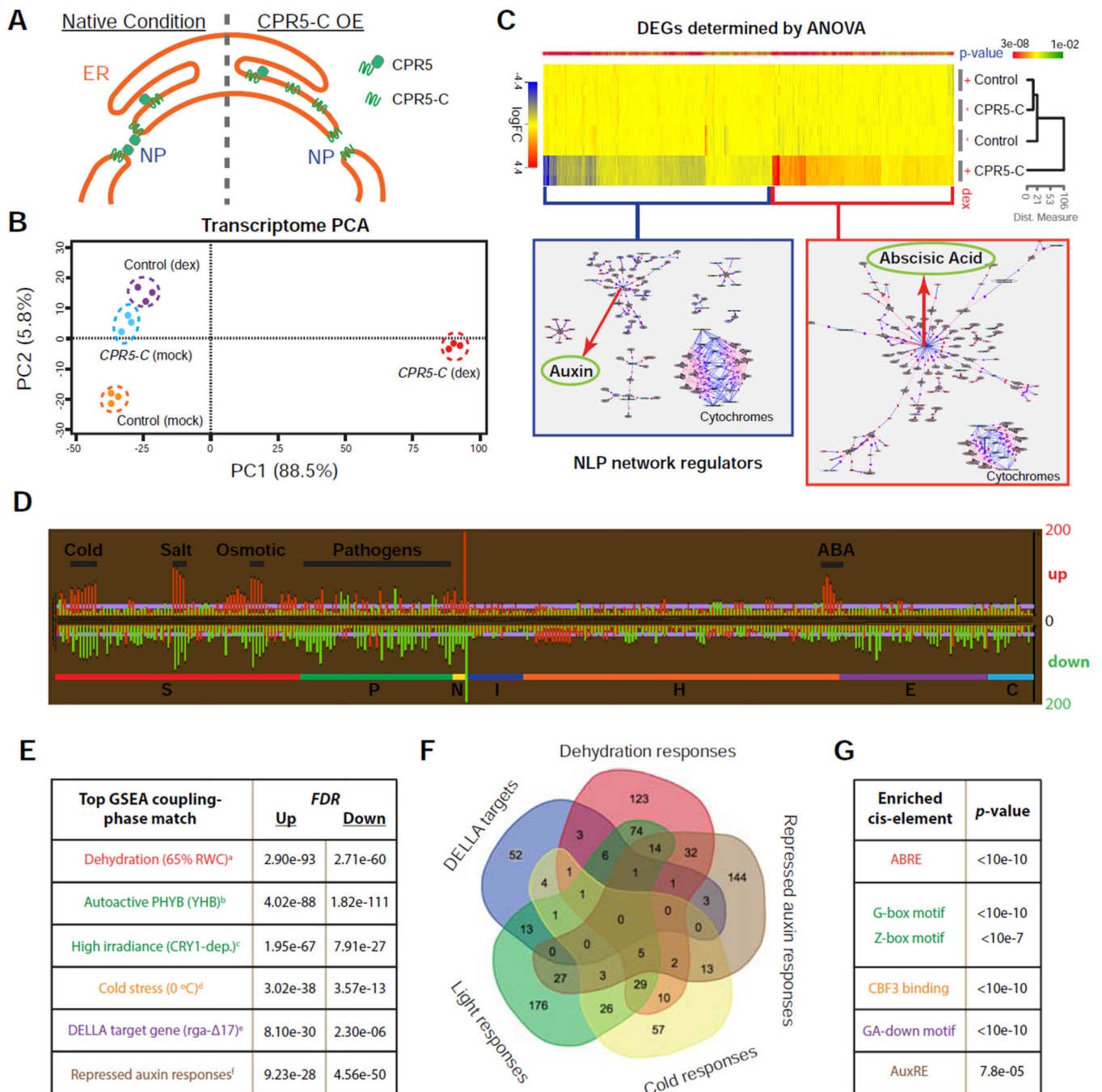


Figure 3. Transient Interference with CPR5 Function Simultaneously Activates Diverse Nuclear Signaling Pathways

(A) A proposed cellular mechanism for transient interference of CPR5 function by overexpression of CPR5-C. NP, nuclear pore.

(B) Principal component analysis (PCA) of transcriptome changes induced by transient expression of CPR5-C.

(C) Heat map of differentially expressed genes (DEGs) that depend on *CPR5-C* transgene induction (p -value < 0.01). Genes with fold change (dex vs mock) higher than 2 were

subject to natural language processing (NLP)-based network regulator discovery analysis. Major network regulators are highlighted with red arrows.

(D) Comparative analysis of CPR5-C-mediated CPR5 interference data with 438 published *Arabidopsis* microarrays. Each row represents an analysis with a specific array dataset, and datasets are sub-categorized into sections according to treatments. Section code: S, stress; P, pathogen; N, nutrient; I, inhibitor; H, hormone; E, elicitor; C, chemical. The length of each bar represents the number of overlapping DEGs (up- or down-regulated) between the CPR5-C data and a specific treatment.

(E) Gene Set Enrichment Analysis (GSEA). CPR5-C-induced up- and down-regulated genes were used as separate inputs for GSEA and non-redundant top matches are listed. PubMed IDs for the listed datasets are: a-21050490, b-19529817, c-17478635, d-16214899, e-17933900, f-19392692.

(F) Venn diagram of the transcriptome signatures identified in (E).

(G) Cis-element enrichment analysis of CPR5-C-induced total DEGs. ABRE, ABA-responsive element; G/Z-box, light-responsive elements; CBF3, transcription factor for cold acclimation; GA-down, gibberellin down regulated d1 cluster; AuxRE, auxin response element.

See also Figure S3 and Table S1.

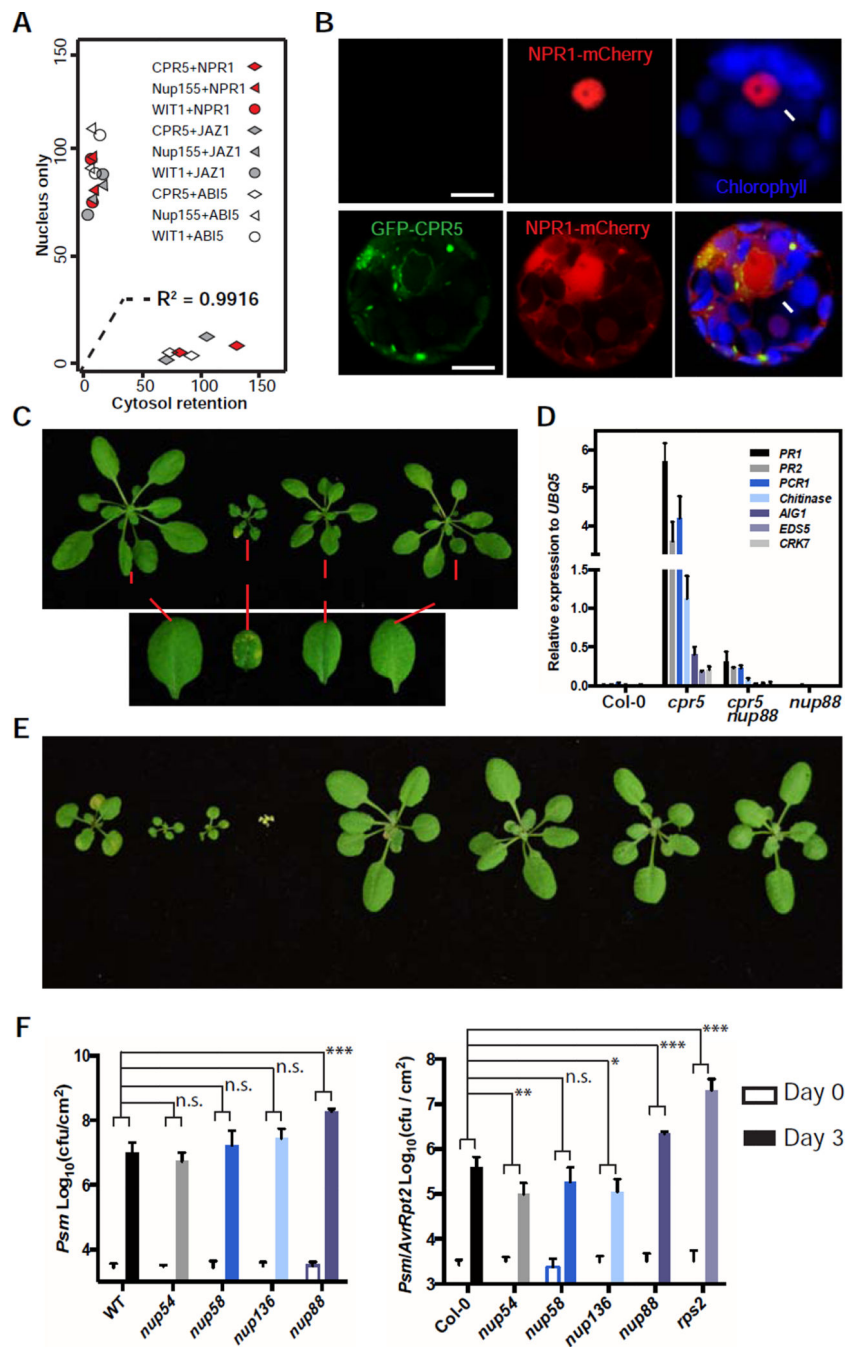


Figure 4. CPR5 Modulates Protein Nucleocytoplasmic Transport to Gate ETI

(A) Overexpression of CPR5 resulted in cytosolic retention of nuclear proteins. NPR1, JAZ1 or ABI5 were co-expressed with NPC protein CPR5, Nup155 or WIT1 in *Arabidopsis* protoplasts. Each combination was repeated twice with around 100 transformed cells counted per repeat. Localization of nuclear proteins in each cell was recorded as binary data ('nucleus only' or 'cytosol retention'). A logistic regression model using the NPC protein as the sole independent variable explains 99% of the data variance.

(B) Representative *Arabidopsis* protoplasts co-transformed with NPR1-mCherry and GFP-CPR5 constructs or the empty vector.

(C) Four-week-old WT, *nup88* (also known as *mos7-1*), *cpr5* and *nup88 cpr5* plants are shown. The lower panel shows close-ups of leaves with or without spontaneous PCD.

(D) Expression levels of the most induced defense-related genes in the *cpr5* mutant were measured using quantitative RT-PCR.

(E) Three-week-old WT, *cpr5*, *cpr5 nup54*, *cpr5 nup58*, *cpr5 nup136*, *nup54*, *nup58* and *nup136* plants.

(F) FG-Nup mutants *nup54* and *nup136* specifically enhanced ETI, but not basal immunity. Three-week-old plants were inoculated with bacterial pathogen *Pseudomonas syringae* pv. *maculicola* (*Psm*) without (left) or with (right) the effector gene *AvrRpt2*. Data are presented as mean \pm SDM (n = 6 biological replications for each genotype and treatment). Two-way ANOVA was used for statistical tests. *p*-values * < 0.05, ** < 0.01, *** < 0.001, n.s. not significant.

See also Figure S4.

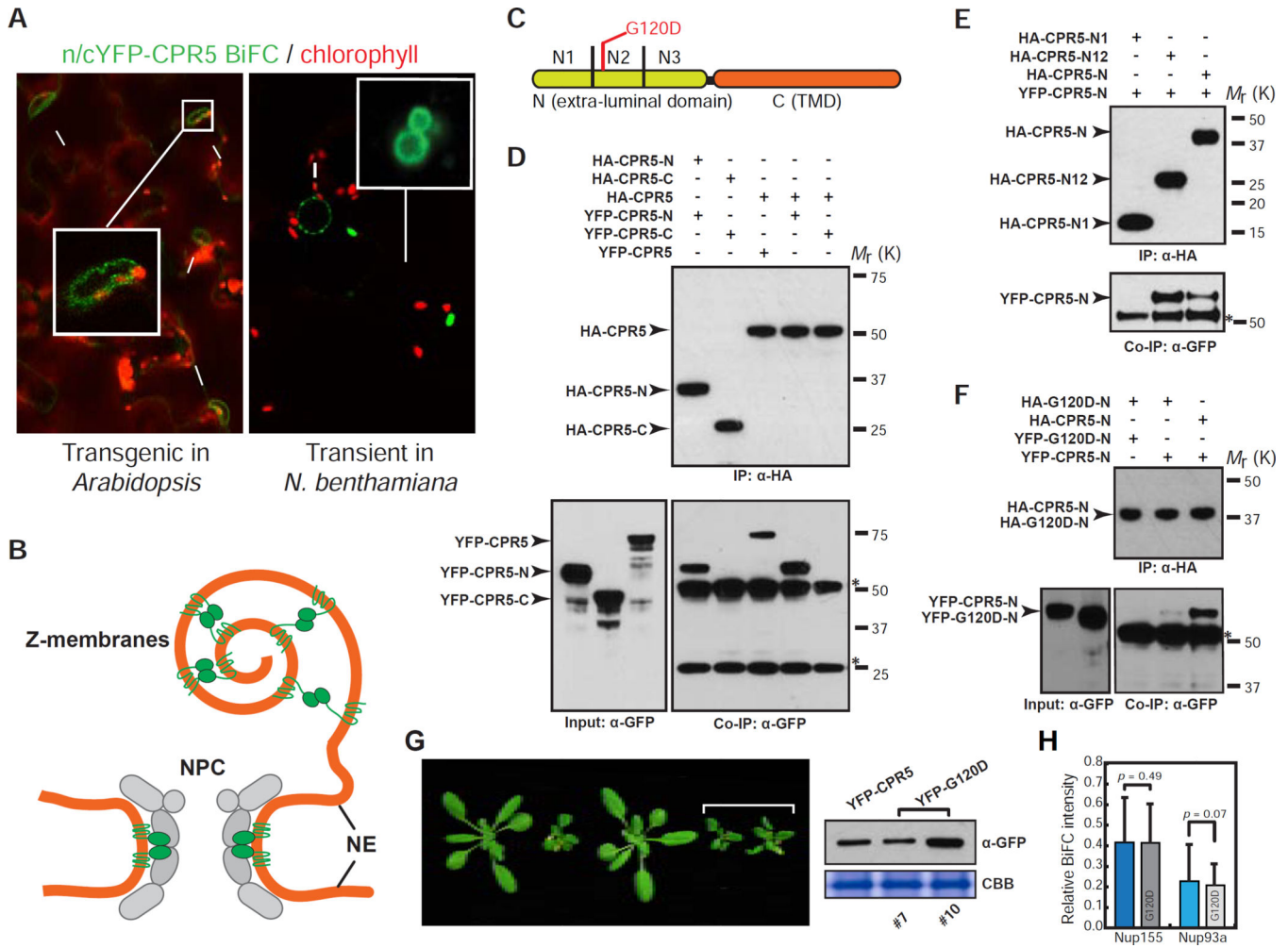


Figure 5. CPR5 Homomeric Interaction at the N-Terminal Extra-Luminal Domain Is Required for Suppressing ETI and PCD

(A) CPR5 BiFC assay. *nYFP-CPR5* and *cYFP-CPR5* were constructed in two separate 35S promoter-driven expression cassettes within one vector (*35S:n/c-YFP-CPR5*). BiFC signals were observed in a stable transgenic *Arabidopsis* line (left) and transiently transformed *N. benthamiana* (right), respectively. Arrows and arrowheads indicate the nucleus and Z-membranes, respectively.

(B) A model proposed for CPR5 homomeric interaction in the NPC and Z-membranes.

(C) Schematic of CPR5 constructs used in *in vitro* pull-down assays. CPR5-N (1–274 aa) and CPR5-C (275–564 aa). CPR5-N was further divided into N1 (1–91 aa), N2 (92–182 aa) and N3 (183–274 aa).

(D–F) CPR5 homomeric interaction is mediated by its N-terminal extra-luminal domain.

CPR5-N, rather than CPR5-C, mediated the homomeric interaction (D). The N1 and N2 (N12) domains of CPR5-C is sufficient and the N2 domain is necessary for the interaction (E). The G120D mutation compromised the homomeric interaction of CPR5-N (F). *In vitro*

pull-down assays were performed using HA antibody-conjugated agarose beads. Stars indicate non-specific signals from immunoglobulins.

(G) Homomeric interaction is required for CPR5 function. *35S:YFP-CPR5* fully complemented the *cpr5-1* mutant phenotype but *35S:YFP-G120D* did not (left) when expressed at comparable levels (right). Two independent *35S:YFP-G120D* transgenic lines (#7 and #10) are shown.

(H) The G120D mutation does not affect heteromeric interactions of CPR5 with other nucleoporins. BiFC was performed by transiently coexpressing nYFP-CPR5/G120D pairwise with Nup155/Nup93a-cYFP in *N. benthamiana*. The BiFC intensity was normalized using averaged expression levels of YFP-CPR5/G120D measured in separate experiments and plotted as relative values. Data are presented as mean \pm SDM (n = 15 cells for each BiFC combination). *p*-values were calculated by Student's *t*-test.

See also Figure S5.

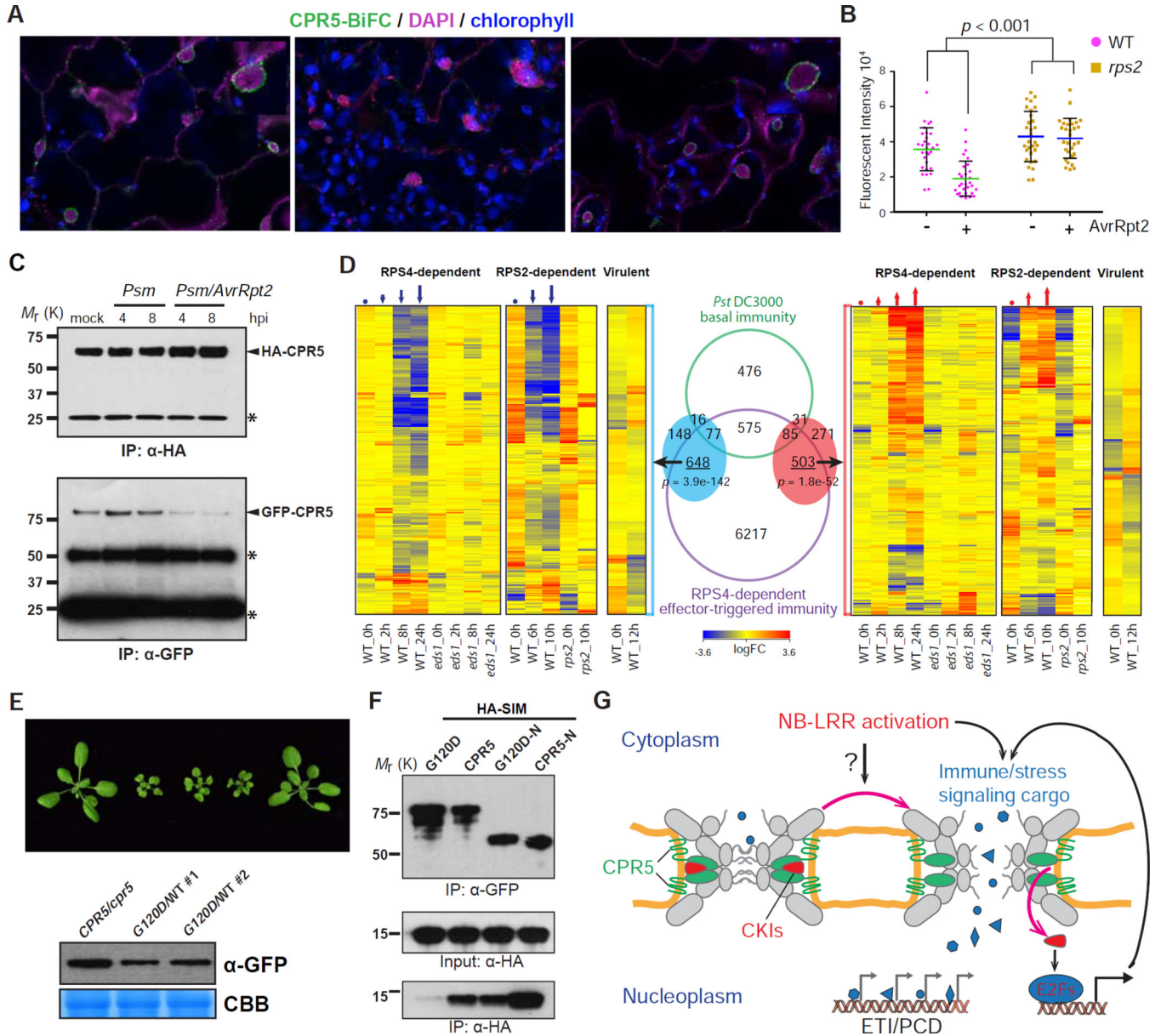


Figure 6. Disruption of CPR5 Homomeric Interaction Is Triggered by NB-LRR Activation and Coordinates CKI-Mediated ETI Signal Transduction and NPC Permeabilization (A–C) ETI-triggered disruption of CPR5 homomeric interaction in the NPC. Leaves of *35S:n/c-YFP-CPR5IDex:AvrRpt2* double transgenic line were incubated with mock or 50 μ M dex for 6–8 hrs before imaging (A). DAPI stained nuclei (arrowheads). BiFC intensities in the NE were measured (B). Data are presented as mean \pm SDM (n = 30 cells for each genotype and treatment). Statistical test was performed using 2-way ANOVA. Total protein was extracted from *35S:GFP-CPR5/HA-CPR5* double transgenic plants treated with *Psm* at indicated time points. Immunoprecipitation was performed using anti-HA agarose beads in the presence of high concentration of detergents (C). hpi, hours post inoculation. (D) CPR5 interference transcriptome shows a significant overlap and concordant expression pattern with those of ETI. Overlaps between CPR5-C-induced (red oval) and repressed (blue

oval) genes with .KRS[^]-dependent ETI genes and basal immunity genes are shown in Venn diagram. Hypergeometric tests were used to calculated-values.

(E) *35S:YFP-G120D* caused dominant negative phenotype in WT plants. Two independent transgenic lines (#1 and #2) and their expression levels are shown.

(F) CPR5 homomeric interaction is required for interaction with SEVI. CPR5/G120D was tagged with YFP and SEVI was tagged with HA. *In vitro* pull-down assay was performed using GFP-TrapA beads.

(G) Permeabilization of the NPC is a specific induction mechanism of ETI and PCD. Upon NB-LRR activation, an unknown intracellular signal is generated and transduced to the NPC to promote the disruption of CPR5 oligomer. This NPC change coordinates CKIs release for ETI signaling and reconfigures the selective barrier to allow significant influx of nuclear signaling cargos through the NPC. These combined effects result in simultaneous activation of diverse stress-related nuclear signaling pathways that contribute to ETI/PCD.

See also Figure S6.